Scaling of the Fock-space propagator and multifractality across the many-body localization transition

Jagannath Sutradhar,[1,*,†] Soumi Ghosh,[1,2,*,‡] Sthitadhi Roy,[2,3,4,§] David E. Logan,[3,5,‖] Subroto Mukerjee,[1,¶] and Sumilan Banerjee[1,**]

[1]*Centre for Condensed Matter Theory, Department of Physics, Indian Institute of Science, Bangalore 560012, India*
[2]*International Centre for Theoretical Sciences, Tata Institute of Fundamental Research, Bengaluru 560089, India*
[3]*Physical and Theoretical Chemistry, Oxford University, South Parks Road, Oxford OX1 3QZ, United Kingdom*
[4]*Rudolf Peierls Centre for Theoretical Physics, Clarendon Laboratory, Oxford University, Parks Road, Oxford OX1 3PU, United Kingdom*
[5]*Department of Physics, Indian Institute of Science, Bangalore 560012, India*

(Received 23 March 2022; revised 31 July 2022; accepted 1 August 2022; published 10 August 2022)

We implement a recursive Green's function method to extract the Fock space (FS) propagator and associated self-energy across the many-body localization (MBL) transition, for one-dimensional interacting fermions in a random on-site potential. We show that the typical value of the imaginary part of the local FS self-energy, Δ_t, related to the decay rate of an initially localized state, acts as a probabilistic order parameter for the thermal to MBL phase transition and can be used to characterize critical properties of the transition as well as the multifractal nature of MBL states as a function of disorder strength W. In particular, we show that a fractal dimension D_s extracted from Δ_t jumps discontinuously across the transition, from $D_s < 1$ in the MBL phase to $D_s = 1$ in the thermal phase. Moreover, Δ_t follows an asymmetrical finite-size scaling form across the thermal-MBL transition, where a nonergodic volume in the thermal phase diverges with a Kosterlitz-Thouless–like essential singularity at the critical point W_c and controls the continuous vanishing of Δ_t as W_c is approached. In contrast, a correlation length (ξ) extracted from Δ_t exhibits a power-law divergence on approaching W_c from the MBL phase.

DOI: 10.1103/PhysRevB.106.054203

I. INTRODUCTION

A many-body localized (MBL) phase is a fascinating nonequilibrium state of matter which can originate in isolated quantum systems in the presence of disorder and interactions [1–4]. In the MBL phase, high-energy eigenstates violate the eigenstate thermalization hypothesis (ETH) [5–7], and local memory can be retained up to arbitrarily long times under time evolution. After the early landmark papers [8,9], a mathematical proof [10] and numerous numerical studies [11–16] have provided strong evidence in favor of the existence of the MBL phase in one dimension. However, the universal properties of the transition from the thermal or ETH phase to the MBL phase remain under active debate [17–23]. This is mainly due to the challenge to "first principles" numerical verification of theoretical scenarios, posed by the exponentially growing Fock-space dimension ($\mathcal{N}_F$) with system size L [11,13,17,24,25]. To complement calculations on microscopic models, several phenomenological renormalization group-based approaches have been employed [18,26–28], which suggest a Kosterlitz-Thouless (KT) -like scenario for the MBL transition.

A further complementary approach to MBL is to consider it as an effective "Fock-space (FS) localization" problem of a fictitious particle on the complex, correlated FS graph (or "lattice") [16,29–31]. This has led to crucial insights such as the role of strong FS correlations in stabilizing the MBL phase [30–33], multifractality of eigenstates therein [17,34–37], and, importantly, a numerical scaling theory of the MBL transition in terms of FS inverse participation ratios (IPR) of eigenstates, which is consistent with a KT-like scenario [35,36]. Here we ask the following question: can a scaling theory of the MBL transition be formulated in terms of FS propagators?

In this work we answer this question in the affirmative, by studying the propagator or Green's function on the FS lattice for a fermionic chain with $L \leqslant 22$. In particular, we extract the local Feenberg self-energy [30,38,39] from the diagonal elements of the FS propagator. As known since Anderson's seminal paper [40], the typical value of the imaginary part of the Feenberg self-energy, Δ_t, acts as a probabilistic order parameter in the thermodynamic limit for Anderson transitions [40–43]. This quantity has recently been employed to construct a self-consistent mean-field theory of the MBL transition on the Fock space [30,31]. However, numerically exact evaluation of the FS self-energy for the microscopic models of MBL, and analysis of its behavior across the MBL transition,

*These authors contributed equally to this work.
† sjagannath@iisc.ac.in
‡soumighosh@alum.iisc.ac.in
§sthitadhi.roy@icts.res.in
‖david.logan@chem.ox.ac.uk
¶smukerjee@iisc.ac.in
**sumilan@iisc.ac.in

is scarce. Here we fill this void and show that the MBL transition from ergodic extended states in the thermal phase to multifractal states in the MBL phase [17,34–37,44–46] is manifest in an anomalous scaling of Δ_t with the Fock-space dimension. This, together with a scaling theory of the MBL transition based on the order parameter Δ_t, that is consistent with the KT-like scenario, constitutes the central result of the work.

The FS propagator contains information about the ergodic/nonergodic nature of the phase, as different eigenstates contribute to it, based on their energy and amplitudes over FS lattice sites. From a technical point of view, computation of the propagator in principle requires all eigenstates. This restricts the system sizes accessible to numerical exact diagonalization (ED), which for $L > 18$ can access only a limited number of eigenstates [47]. To access larger sizes, comparable to those accessible via parallelized shift-invert method [47] or POLFED [48], but at significantly cheaper computational cost, we compute the FS propagators using a standard recursive Green's function method [49–51], but adapted to the FS graph. Moreover, for the reasons discussed below, we study a scaled version of the self-energy, viz. $\Delta_t/\sqrt{L}$, and refer to it as Δ_t throughout the rest of the paper for notational convenience. Employing the recursive method, we obtain the following main results.

(1) The typical value Δ_t of the self-energy is finite in the thermal phase. It vanishes $\propto \mathcal{N}_F^{-(1-D_s)}$ in the MBL phase and at the critical point, where $D_s < 1$ is a fractal dimension reflecting the multifractal nature of the states. D_s changes discontinuously across the MBL transition, from $D_s < 1$ to $D_s = 1$ throughout the thermal phase.

(2) The finite-size scaling of Δ_t as a function of disorder strength (W) is consistent with an asymmetric finite-size scaling form [35,36,52,53] across the MBL transition. Scaling on the thermal side is controlled by a nonergodic volume scale Λ, which diverges with an essential singularity $\Lambda \sim \exp(b/\sqrt{\delta W})$ [$\delta W = (W_c - W)$, $b \sim O(1)$] at a critical disorder (W_c), redolent of a KT-like transition. Scaling on the MBL side by contrast is controlled by a FS correlation length (ξ), which exhibits a power-law divergence on approaching criticality. Moreover, the scaling theory implies that in the thermodynamic limit Δ_t vanishes continuously on approaching the transition from the thermal side as $\sim \exp[-b'/\sqrt{\delta W}]$ with $b' \sim O(1)$.

As already mentioned, multifractal characterization of MBL states [17,34] and numerical scaling theory consistent with a KT-like MBL transition have been obtained via study of eigenstate IPRs [35,36]. However, our work reveals the multifractality and KT-type critical scaling in terms of a FS order parameter for the thermal-MBL transition. Additionally, the FS order parameter, being associated with an inverse decay time of localized initial states, provides a truly dynamical characterization of MBL transition unlike the static properties studied based on eigenstates in the previous studies [17,34–36].

II. MODEL

We study the following standard model [11–13,15–17,54] of MBL for a fermionic chain with an i.i.d. random on-site potential $\epsilon_i \in [-W, W]$ of strength W on $i = 1, \ldots, L$ sites and nearest-neighbor repulsion (V),

$$\mathcal{H} = t \sum_{i=1}^{L-1} \left(c_i^\dagger c_{i+1} + c_{i+1}^\dagger c_i \right) + \sum_{i=1}^{L} \epsilon_i \hat{n}_i + V \sum_{i=1}^{L-1} \hat{n}_i \hat{n}_{i+1}. \quad (1)$$

Here $c_i^\dagger$ (c_i) is the fermion creation (annihilation) operator for site i, with number operator $\hat{n}_i = c_i^\dagger c_i$. We choose $t = 0.5$ and $V = 1$ to be consistent with earlier studies and study the model in the half-filled sector at "infinite temperature," which corresponds to the middle of the many-body energy spectrum. In this case, the model shows a thermal to MBL transition at a critical disorder $W_c \simeq 3.7$–4.2 [17]. In this work, we take the critical disorder W_c as 3.75. Variation of W_c between $\sim$3.5 and 4 leads to comparably good scaling collapse in our finite-size scaling analysis.

To describe the many-body system in Fock space, we employ the occupation-number basis $\{|I\rangle\}$ of particles on the real-space sites, $|I\rangle = |n_1^{(I)} n_2^{(I)} \ldots n_L^{(I)}\rangle$ with $n_i^{(I)} \in 0$ or 1. In this basis, the Hamiltonian Eq. (1) takes the form of a tight-binding model [30,33,55]

$$\mathcal{H} = \sum_{I,J} T_{IJ} \, |I\rangle \langle J| + \sum_I \mathcal{E}_I \, |I\rangle \langle I| \,, \quad (2)$$

but on the FS lattice [Fig. 1(a)]. Here, the FS "hopping" $T_{IJ} = t$ when $|I\rangle$ and $|J\rangle$ are connected by a single nearest-neighbor hop in real space and $T_{IJ} = 0$ otherwise. The on-site "disorder" potential at FS site I is $\mathcal{E}_I = \sum_i \epsilon_i n_i^{(I)} + V \sum_i n_i^{(I)} n_{i+1}^{(I)}$, and is a combination of the real-space disorder potential and the nearest-neighbor interaction.

The disorder-averaged many-body density of states for the model is a Gaussian as a function of energy E, with the mean

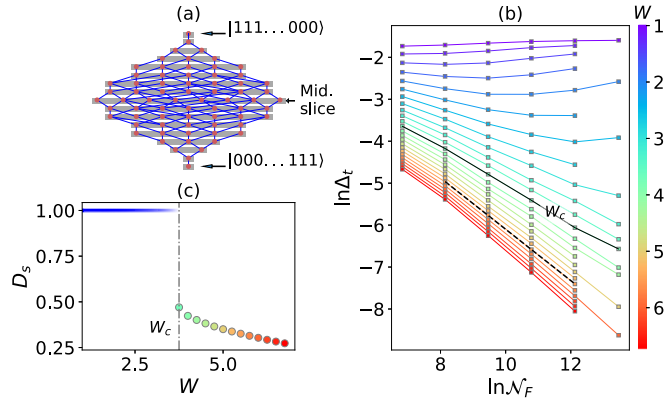

FIG. 1. (a) Fock-space lattice constructed out of real-space occupation-number basis states (orange circles), illustrated for $L = 8$, starting at the top with $|111...000\rangle$, i.e., all particles on the left side, and ending at the bottom with all particles on the right. The hoppings (blue lines) and the slices (gray lines) are indicated. (b) $\ln \Delta_t$ as a function of $\ln \mathcal{N}_F \propto L$ for different W (color bar) across the MBL transition (W_c). The exponential decrease of Δ_t with L for $W > W_c$ is shown by the dashed black line (linear fit) for one value of W. We also show the data for $L = 22$ for several disorder strengths. (c) The fractal dimension D_s obtained from the finite-size scaling theory jumps discontinuously across the transition, from $D_s < 1$ in the MBL phase to $D_s = 1$ in the thermal phase. At $W = W_c$ (vertical dash-dotted line) $D_s \simeq 0.5$.

$\propto L$ and variance $\mu_E^2 = (t^2 + W^2/6 + V^2/8)L/2$ [55]. As a result, to treat different system sizes on the same footing and for the theory to have a well-defined thermodynamic limit [31], we scale the parameters and work with a rescaled $\tilde{\mathcal{H}} = \mathcal{H}/\sqrt{L}$ [30,31,55]. This leads directly to the scaled version of the self-energy mentioned above. We also set the mean many-body energy to zero, by transforming $\tilde{\mathcal{H}}$ to $\tilde{\mathcal{H}} - \mathbb{1}\,\mathrm{Tr}\tilde{\mathcal{H}}/\mathcal{N}_F$ for each disorder realization, since the middle of the spectrum fluctuates with disorder realization for a finite system.

III. RECURSIVE GREEN'S FUNCTION METHOD

Elements of the retarded FS propagator $G(E) = [(E + i\eta)\mathbb{1} - \tilde{\mathcal{H}}]^{-1}$ are computed by implementing the standard recursive method [49–51,56,57] at the middle ($E = 0$) of the energy spectrum. We choose the broadening (or regulator) $\eta(W) = \sqrt{2\pi}\mu_E/(\sqrt{L}\mathcal{N}_F)$ [30,55], the mean many-body level spacing of $\tilde{\mathcal{H}}$, which depends on disorder strength W through the variance μ_E^2. We arrange the Fock space basis states in a layered lattice structure, as illustrated in Fig. 1(a). Crucially, this is local, in that sites belonging to any slice or layer are connected through hopping only to sites belonging to the nearest-neighbor layers. It is this locality that allows for an efficient implementation of the method for the FS lattice, as detailed in Appendix A.

We calculate the diagonal elements $G_{II}(E) = \langle I|G(E)|I\rangle$, where $I \in$ the middle slice M [Fig. 1(a)]. We extract one of the important characterizations of the localization properties in the FS, the imaginary part Δ_I of the Feenberg self-energy $\Sigma_I(E) = X_I(E) - i\Delta_I(E) \equiv G_{II}^{-1}(E) - (E + i\eta - \mathcal{E}_I)$ at a FS site I. As mentioned in the Introduction, the analogous quantity on the real-space lattice was quintessential in the development of the concept of localization [40] for noninteracting systems. We consider the distributions of Δ_I, in particular its disorder-averaged typical value, denoted by Δ_t. The latter is the geometric mean calculated by averaging over different disorder realizations and different Fock space sites using $\ln \Delta_t = \langle \ln \Delta_I\rangle_{I,\{\epsilon_i\}}$, where $\langle \ldots\rangle_{I,\{\epsilon_i\}}$ denotes averaging over $I \in M$ and disorder realizations $\{\epsilon_i\}$. Depending on L, $\sim$150 to 10 000 disorder realizations are employed to generate the distribution of Δ_I (Appendix C). We have checked that our results converge with the number of disorder samples for all the system sizes, $L = 12$–22, that we study, and the details are given in Appendix C.

IV. MULTIFRACTALITY AND SCALING THEORY FROM THE IMAGINARY PART OF FEENBERG SELF-ENERGY

The imaginary part $\Delta_I(E)$ of the self-energy determines the energy-resolved decay time $[\Delta_I(E)^{-1}]$ of a localized initial state $|I\rangle$ or, alternatively, the lifetime of an excitation with energy E created at the FS lattice site I [40]. As such, $\Delta_I(E)$ directly encodes information about localization or lack thereof. In the thermal phase, the typical value $\Delta_t \sim O(1)$, as the initial state decays in a finite time, whereas, in the MBL phase, $\Delta_t \to 0$ in the thermodynamic limit $\mathcal{N}_F \to \infty$.

Numerical results for Δ_t as a function of $\mathcal{N}_F$ are shown in Fig. 1(b). Δ_t indeed decreases as a function of W from an $O(1)$ value in the thermal phase to a value which in the MBL phase vanishes exponentially rapidly with L. Deep in the thermal phase at weak disorder, Δ_t is independent of $\mathcal{N}_F$. By contrast, in the MBL phase ($W > W_c$), Δ_t decays as a power law, $\propto \mathcal{N}_F^{-(1-D_s)}$ with $0 < D_s < 1$. As discussed later, D_s is a spectral fractal dimension which characterizes the multifractality of the MBL states. It depends on W as shown in Fig. 1(c), where D_s has been obtained from the finite-size scaling analysis discussed below. Note that, at intermediate disorder in the ETH phase, Δ_t initially decays with $\mathcal{N}_F$ for small L, before showing an increasing trend, presumably towards its finite asymptotic value in the thermodynamic limit [Fig. 1(b)]. This indicates that the systems are in the critical regime at intermediate disorder.

The bare data itself conforms to the expectation that in the thermodynamic limit Δ_t vanishes in the MBL phase and approaches a finite $O(1)$ value in the thermal phase. But to analyze compellingly the critical properties of Δ_t, we perform a scaling collapse of the data using the following finite-size scaling ansatz [35,36,52]:

$$\ln \frac{\Delta_t}{\Delta_c} = \begin{cases} \mathcal{F}_{\mathrm{vol}}\left(\frac{\mathcal{N}_F}{\Lambda}\right): & W < W_c, \\ \mathcal{F}_{\mathrm{lin}}\left(\frac{\ln \mathcal{N}_F}{\xi}\right): & W > W_c, \end{cases} \tag{3}$$

where $\Delta_c = \Delta_t(W = W_c) \sim \mathcal{N}_F^{-(1-D_c)}$. The scaling ansatz states that, in the ETH phase, Δ_t follows a "volumic" scaling form where the finite-size scaling is controlled by a Fock-space volume scale, Λ [35,36,52]. In the MBL phase, on the other hand, the scaling form is "linear" with the scaling controlled by a Fock-space length scale, ξ [35,36,52]. Taking $W_c = 3.75$, the good collapse of the data shown in Fig. 2 suggests that the above scaling forms are appropriate. As shown in Appendix B, varying W_c between $\sim$3.5 and 4 leads to comparably good scaling.

The "nonergodic" volume $\Lambda(W)$ [52] extracted from the scaling collapse of $\ln(\Delta_t/\Delta_c)$ in the thermal phase ($W < W_c$) is shown in the upper panel of Fig. 2 (inset). Λ diverges at the critical point with a KT-like essential singularity, $\Lambda \sim \exp[b/(\delta W)^\alpha]$ with $\alpha \simeq 0.5$, where $\delta W = (W_c - W)$ and $b \sim O(1)$. This kind of KT-type singularity has been predicted by a phenomenological RG theory [18,26–28], albeit based on a real-space picture. Throughout the ETH phase, since the eigenstates are understood to be ergodic [35], we expect $\Delta_t \sim O(1)$ asymptotically in the limit $\mathcal{N}_F \gg \Lambda$. This implies for the volumic scaling function in Eq. (3) that $\mathcal{F}_{\mathrm{vol}}(x) \sim (1 - D_c)\ln x$ for $x \gg 1$. As evinced in the upper panel of Fig. 2, this is indeed the asymptotic form of the scaling function, $\mathcal{F}_{\mathrm{vol}}(x) \sim 0.49\ln x$ (see Appendix B for details) from which we estimate $D_c \simeq 0.51$. This is an excellent agreement with $D_c \simeq 0.5$ obtained by fitting the raw data of Δ_t against $\mathcal{N}_F$ for $W_c = 3.75$ [Fig. 1(b)]. A significant conclusion from this is that $D_s = 1$ throughout the ETH phase and jumps *discontinuously* to a value $D_s < 1$ at the MBL transition, whereafter it decreases smoothly with increasing W [Fig. 1(c)]. This is in complete consonance with the discontinuity across the MBL transition of the fractal dimension characterizing the Fock-space IPRs of the eigenstates [35,36]. Furthermore, the form of the divergence of Λ and the asymptotic form of $\mathcal{F}_{\mathrm{vol}}$ implies that, in the thermodynamic limit, Δ_t vanishes continuously as the transition is approached from the ETH side as $\Delta_t \sim \Lambda^{-(1-D_c)} \sim \exp[-b(1 - D_c)/\delta W^\alpha]$.

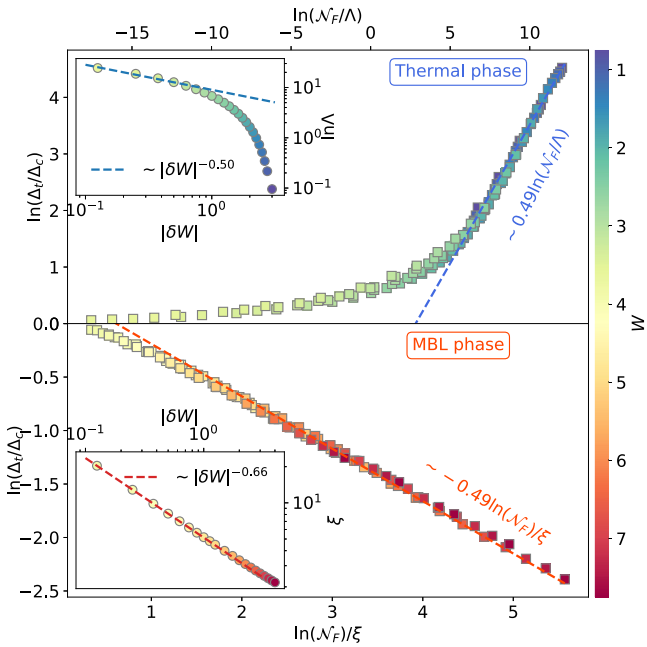

FIG. 2. Finite-size scaling collapse of $\ln(\Delta_t/\Delta_c)$ using respectively the volumic and linear scaling [Eq. (3)] in the thermal (upper panel) and MBL (lower panel) phase, with $W_c = 3.75$. *Upper panel*: the asymptotic scaling of $\ln(\Delta_t/\Delta_c) \sim 0.5 \ln(\mathcal{N}_F/\Lambda)$ deep in the thermal phase is determined by the exponent $(1 - D_c) \simeq 0.5$ at $W = W_c$, where $\Delta_c \sim \mathcal{N}_F^{-(1-D_c)}$. Inset shows the KT-like essential singularity of the nonergodic volume, $\Lambda \sim \exp(b/\sqrt{\delta W})$ with $\delta W = (W_c - W)$, near W_c. *Lower panel*: deep in the MBL phase, asymptotic scaling gives $\ln(\Delta_t/\Delta_c) \propto (\ln \mathcal{N}_F)/\xi$. The inset shows the divergence of the correlation length, $\xi \sim |\delta W|^{-\beta}$ with $\beta \simeq 0.7$, on approaching the transition from the MBL phase. System sizes from $L = 12$ to 20 were used to obtain the scaling.

In the MBL phase for $W > W_c$, the scaling collapse yields a diverging correlation length, $\xi \sim (W - W_c)^{-\beta}$ with $\beta \simeq 0.7$, as shown in the lower panel of Fig. 2 (inset). For $x = (\ln \mathcal{N}_F)/\xi \gg 1$, the asymptotic scaling is $\mathcal{F}_{\rm lin}(x) \sim -(1 - D_c)x$ (Appendix B), as indeed seen in Fig. 2, lower panel. From the form of $\mathcal{F}_{\rm lin}(x)$, $\xi = (1 - D_c)/(D_c - D_s)$, which implies a divergent ξ as $D_s \to D_c$, i.e., $W \to W_c+$ (Appendix B). Note that $D_c < 1$ implies that the MBL critical point is actually a part of the MBL phase itself. This is consistent with the understanding that the entire MBL phase is critical in the sense that it is multifractal, and the MBL transition can be understood as the terminal end point of the line of fixed points.

Having established the critical scaling of the FS order parameter Δ_t and the volume (length) scale in the thermal (MBL) phase, we now discuss how the system-size scaling $\Delta_t \sim \mathcal{N}_F^{-(1-D_s)}$ in Figs. 1(b) and 1(c) for $W > W_c$ is related to multifractality in the MBL phase. MBL eigenstates are known to be multifractal in nature [17,34–37], i.e., nonergodic but extended over $\sim \mathcal{N}_F^D$ $(0 < D < 1)$ FS sites. Similar to the case of the local density of states discussed in Ref. [58], the multifractality can be deduced from the dependence of the typical value and the distribution of Δ_I, on the broadening parameter η for large but finite $\mathcal{N}_F$. In this limit, Δ_t saturates as

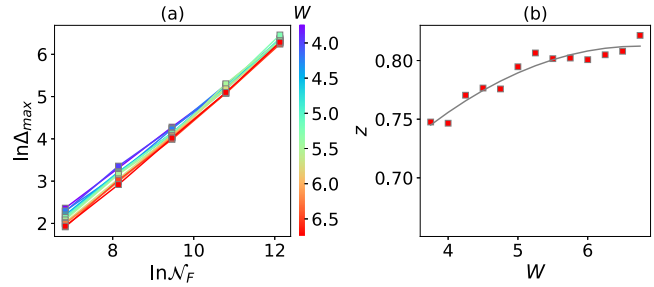

FIG. 3. (a) In the MBL phase, the scaling of $\Delta_{\rm max}$ with the Fock space dimension $\mathcal{N}_F$ is shown to follow a power-law $\Delta_{\rm max} \propto \mathcal{N}_F^z$ for different disorder strengths (color bar). To obtain good statistics, $\ln \Delta_{\rm max}$ plotted here is averaged over a few of the largest values of $\ln \Delta$ for a given L and W. (b) The exponent z, obtained from $\Delta_{\rm max} \sim \eta_c^{-1} \sim \mathcal{N}_F^z$ in (a), is shown to be <1 in the MBL phase, consistent with the multifractal scaling of the self-energies. The solid line is merely a guide to the eye.

a function of η below an energy scale $\eta_c \sim \mathcal{N}_F^{-z}$ $(0 < z < 1)$, namely, $\Delta_t \sim \eta_c^\theta \sim \mathcal{N}_F^{-(1-D_s)}$ for $\eta \ll \eta_c$, whereas $\Delta_t \sim \eta^\theta$ for $\eta \gg \eta_c$. Here the exponent $\theta > 0$ and the spectral fractal dimension $D_s = 1 - z\theta$ lies between 0 and 1 [58]. Physically, η_c signifies the presence of an energy scale much larger than the mean level spacing $\mathcal{N}_F^{-1}$ for multifractal states for any finite system. In our calculations, $\eta \propto \mathcal{N}_F^{-1} \ll \eta_c$; thus we expect $\Delta_t \sim \mathcal{N}_F^{-(1-D_s)}$. This is indeed the behavior for $\Delta_t(\mathcal{N}_F)$ that we find in Fig. 1(b) over the entire MBL range $(W > W_c)$. It is also completely consistent with the asymptotic form of the scaling function [Fig. 2 (lower panel)] and the D_s extracted from it [Fig. 1(b)]. The spectral dimension D_s can be shown to be the same as the fractal dimension D extracted from the eigenstates under very general considerations [58]. We note that the behavior $\Delta_t \sim \mathcal{N}_F^{-(1-D_s)}$ is different from a self-consistent theory [30,31] of MBL, where the thermodynamic limit of $\mathcal{N}_F \to \infty$ is taken first before taking the $\eta \to 0$ limit. As a result, one obtains $\Delta_t \propto \eta$ and such a theory does not in effect distinguish between Anderson localized and multifractal states.

Further insight into the multifractal behavior may be gained by analyzing the tail of the probability distribution function $P(\Delta)$ of Δ_I over disorder realizations. For finite η and/or $\mathcal{N}_F$, one expects [58] the distribution to be cut off at a maximum value $\Delta = \Delta_{\rm max}$, where $\Delta_{\rm max} \sim 1/\eta_c \sim \mathcal{N}_F^z$ for $\eta \ll \eta_c$. As shown in Fig. 3(a), we indeed find that $\Delta_{\rm max}$ directly extracted from the numerical data follows a power law $\sim \mathcal{N}_F^z$. The exponent z extracted from $\Delta_{\rm max}$ is shown in Fig. 3(b) and indeed satisfies $0 < z < 1$. This further confirms the multifractal scaling of the self-energy in the MBL phase.

V. CONCLUSION

Using a recursive Green's function method, we have in summary obtained the critical scaling across the MBL transition by calculating the self-energy associated with the local Fock-space propagator, the typical value of the imaginary part of which, Δ_t, acts as an order parameter for the MBL transition. The finite-size scaling of Δ_t implies the existence of a nonergodic volume with a KT-like essential singularity, which

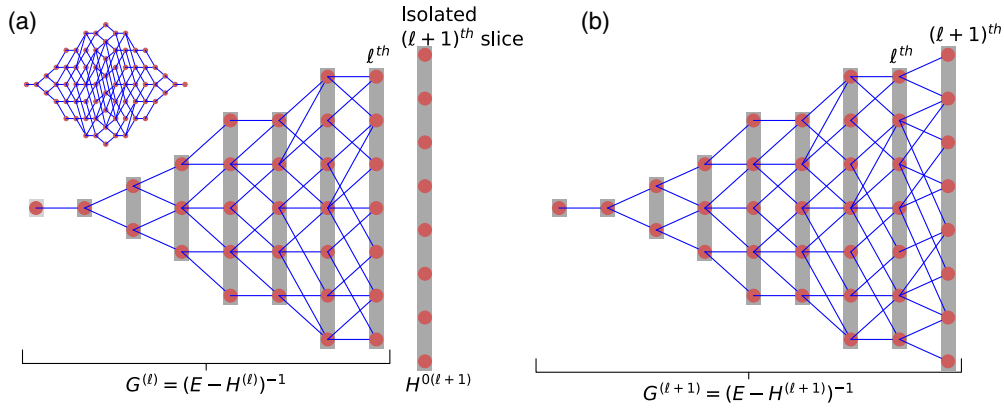

FIG. 4. (a) Figure on the top left corner is similar to Fig. 1(a), but rotated by 90°. The larger figure shows a part of it, up to ℓth slice, where the gray shaded area shows each slice. Orange circles and solid blue lines represent the FS sites and hopping, respectively. (b) As we keep on adding the next slices, the Green's function of the left part gets updated via the iterative Eqs. (A2)

directly controls the continuous vanishing of Δ_t on approach to the transition from the ergodic side and the multifractal nature of the MBL phase was demonstrated via determination of the spectral fractal dimension D_s, which was shown to change discontinuously across the transition. While our focus here has been on the local FS propagator, the recursive Green's function method also gives access to the nonlocal propagator, a question of immediate future interest which can potentially provide insights into the critical scaling of a FS localization length and also enable study of the inhomogeneous nature of MBL eigenstates on the FS lattice [36]. It would also be interesting to explore further the connection [36] between real-space and Fock-space critical properties, e.g., how rare thermal regions in real space [59–61] affect the FS self-energy. In the same vein, possible connections between the Fock-space propagators and one-particle density matrix and real-space propagators [62–67] also remain a question for future work.

ACKNOWLEDGMENTS

S.B. acknowledges support from SERB (Grant No. ECR/2018/001742), DST, India. S.M. acknowledges support from QuST, DST, India. S.R. acknowledges support from an ICTS-Simons Early Career Faculty Fellowship via a grant from the Simons Foundation (Grant No. 677895, R.G.) and EPSRC Grant No. EP/S020527/1.

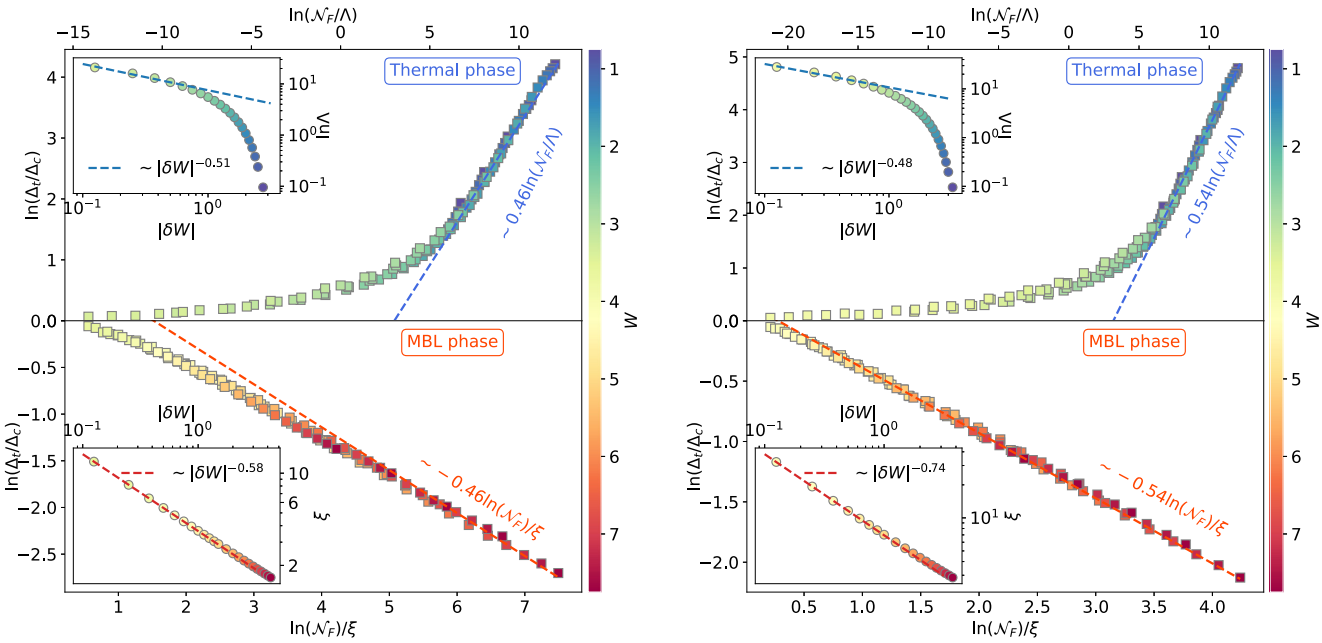

FIG. 5. Finite-size scaling collapse of $\ln(\Delta_t/\Delta_c)$ in direct parallel to that of Fig. 2 for $W_c = 3.75$, but shown here for $W_c = 3.5$ (left panel) and $W_c = 4.0$ (right panel).

APPENDIX A: RECURSIVE GREEN'S FUNCTION METHOD

In the recursive method, we calculate different elements of the Green's function by starting from one of the two minimally connected Fock-space sites ($|111\ldots000\rangle$, $|000\ldots111\rangle$) and by adding the next slice connected by hopping to the earlier slice at each step. Here we start with the top site $|111\ldots000\rangle$ as shown in Fig. 1(a). At each iteration step, the method inverts a matrix containing the Hamiltonian elements for the added slice and is, therefore, of size $\mathcal{N}_\ell \times \mathcal{N}_\ell$, where $\mathcal{N}_\ell$ is the size of the added slice. Hence this method avoids the inversion of the full Hamiltonian in Eq. (2). The maximum size of the matrix $(\mathcal{N}_M \times \mathcal{N}_M)$ that is inverted during the calculation is determined by the number of sites $\mathcal{N}_M$ in the middle slice, which is the largest slice of the Fock space [Fig. 1(a)]. For L between 10 and 22, $\mathcal{N}_M$ is between $\sim$1 and 2 orders of magnitude lower than the full Fock-space dimension $\mathcal{N}_F = \binom{L}{L/2}$. It is this substantial reduction that provides the advantage to achieve the system size $L = 22$ even with serial computation. The method can be applied to even larger systems like $L = 24$ with parallelization.

At the ℓth step of recursion, let $H^{(\ell)}$ be the Hamiltonian corresponding to the part of the Fock space lattice containing all slices up to the ℓth slice. The corresponding Green's function for these ℓ slices is given by $G^{(\ell)} = [E^+\mathbb{1} - H^{(\ell)}]^{-1}$, where $E^+ = E + i\eta$. Using Eq. (2) and the local structure of the Fock space lattice, the Hamiltonian corresponding to all slices up to the $(\ell+1)$th slice can be written as

$$H^{(\ell+1)} = \begin{pmatrix} H^{(\ell)} & \mathcal{T}_{lr} \\ T_{rl} & H^{(0)(\ell+1)} \end{pmatrix},$$

$$H^{(0)(\ell+1)} = \sum_{I\in(\ell+1)} \mathcal{E}_{I,\ell+1}\,|I,\ell+1\rangle\,\langle I,\ell+1|\,,$$

$$\mathcal{T}_{lr} = \sum_{I\in\ell}\sum_{J\in(\ell+1)} T_{I,J}\,|J,\ell+1\rangle\,\langle I,\ell|\,,$$

where $H^{(0)(\ell+1)}$ contains the part of the Hamiltonian corresponding to the $(\ell+1)$th slice disconnected from the rest of the Fock lattice, $\mathcal{T}_{lr}$ contains the hopping elements for hopping from the ℓth slice to the $(\ell+1)$th slice, and $\mathcal{T}_{rl} = \mathcal{T}_{lr}^\dagger$. $|I,\ell\rangle$, representing the state $|I\rangle$, explicitly mentions the slice index ℓ which $|I\rangle$ belongs to. Similarly, the Green's function at the $(\ell+1)$th step can be written as

$$G^{(\ell+1)} = \begin{pmatrix} G_l^{(\ell+1)} & G_{lr}^{(\ell+1)} \\ G_{rl}^{(\ell+1)} & G_r^{(\ell+1)} \end{pmatrix}.$$

Here the subscript l denotes the matrix elements of the left part (first to the ℓth slice) and r denotes the elements of the $(\ell+1)$th slice, as described in Fig. 4. Then, at the $(\ell+1)$th step of recursion, the Green's function $G^{(\ell+1)}$ and the Hamiltonian $H^{(\ell+1)}$ have the following matrix equation:

$$[E^+\mathbb{1} - H^{(\ell+1)}]G^{(\ell+1)} = \mathbb{1},$$

$$\begin{pmatrix} (G^{(\ell)})^{-1} & \mathcal{T}_{lr}, \\ \mathcal{T}_{rl} & (G^{0(\ell+1)})^{-1} \end{pmatrix} \begin{pmatrix} G_l^{(\ell+1)} & G_{lr}^{(\ell+1)} \\ G_{rl}^{(\ell+1)} & G_r^{(\ell+1)} \end{pmatrix} = \mathbb{1}. \quad \text{(A1)}$$

Here $(G^{(\ell)})^{-1} = (E^+\mathbb{1} - H^{(\ell)})$ and $(G^{0(\ell+1)})^{-1}$ is given by $[E^+\mathbb{1} - H^{(0)(\ell+1)}]$. From the above equation, we can obtain

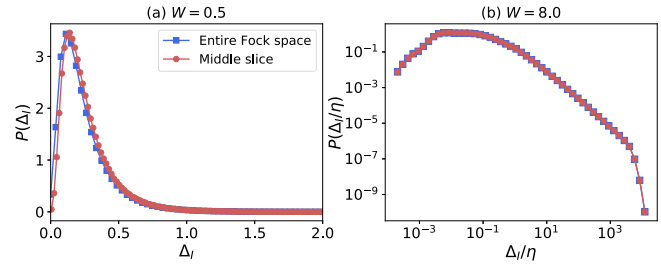

FIG. 6. Probability distributions of the imaginary part Δ_I of the self-energy, considering both $I \in M$ and $I \in$ FS. These match well with each other, in both the thermal phase [shown in (a)] and MBL phase (b). Data shown in the figure are for system size $L = 14$.

the following equation:

$$G_l^{(\ell+1)} = G^{(\ell)} + G^{(\ell)}\mathcal{T}_{lr}G_{rl}^{(\ell+1)},$$

$$\langle s|G_l^{(\ell+1)}|s'\rangle = \langle s|G^{(\ell)}|s'\rangle + \langle s|G^{(\ell)}(\mathbb{T}_\ell|\ell\rangle\langle\ell+1|) \times G_{rl}^{(\ell+1)}|s'\rangle, \quad s,s' \leqslant \ell.$$

Note that $\langle s|A|s'\rangle = A(s,s')$ denotes an element of a rectangular matrix A, as each of the slices, indexed by s and s', contains different numbers of lattice points in general. For the same reason, $\mathbb{T}_\ell$ is also a rectangular matrix containing hopping matrix elements between ℓth and $(\ell+1)$th slices. Therefore,

$$G^{(\ell+1)}(s,s') = G^{(\ell)}(s,s') + G^{(\ell)}(s,\ell)\mathbb{T}_\ell G^{(\ell+1)}(\ell+1,s'), \quad s,s' \leqslant \ell.$$

Similarly, starting from Eq. (A1),

$$G^{(\ell+1)}(\ell+1,s) = G^{(\ell+1)}(\ell+1,\ell+1)\mathbb{T}_\ell^\dagger G^{(\ell)}(\ell,s), \quad s \leqslant \ell, \quad \text{(A2a)}$$

$$G^{(\ell+1)}(s,\ell+1) = G^{(\ell)}(s,\ell)\mathbb{T}_\ell^\dagger G^{(\ell+1)}(\ell+1,\ell+1), \quad s \leqslant \ell. \quad \text{(A2b)}$$

Therefore, for $s, s' \leqslant \ell$,

$$G^{(\ell+1)}(s,s') = G^{(\ell)}(s,s') + G^{(\ell)}(s,\ell)\mathbb{T}_\ell G^{(\ell+1)} \times (\ell+1,\ell+1)\mathbb{T}_\ell G^{(\ell)}(\ell,s'), \quad \text{(A2c)}$$

TABLE I. L and the corresponding number of disorder realizations employed to generate the distributions of Δ_I at each W point are shown in the first two columns. The third column estimates the product of the number of disorder realizations and the number of FS sites in the middle slice.

L	No. of disorder realizations	No. of total data points
12	10^4	6×10^4
14	5×10^3	8×10^5
16	2×10^3	11×10^5
18	10^3	17×10^5
20	500	27×10^5
22	130	23×10^5

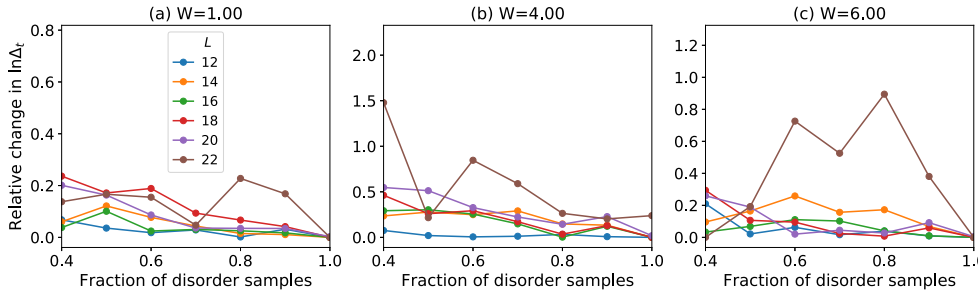

FIG. 7. Relative *percentage* change in $\ln\Delta_t$ as the sample size is changed from 0.4 times the maximum sample size to the maximum sample size. The relative change is defined as $|(\ln\Delta_t - \ln\Delta_t^{(1)})/\ln\Delta_t^{(1)}|$, where $\ln\Delta_t^{(1)}$ is calculated considering all the available samples. This shows the value of $\ln\Delta_t$ is always within 1% of the values plotted in Fig. 1(b) even for smaller sample sizes, and for all system sizes up to $L = 22$.

and on-slice elements

$$G^{(\ell+1)}(\ell+1,\ell+1) = [(G^{0(\ell+1)})^{-1} - \underbrace{\mathbb{T}_\ell^\dagger G^{(\ell)}(\ell,\ell)\mathbb{T}_\ell}_{\text{self-energy } \Sigma^{(\ell)}}]^{-1}. \tag{A2d}$$

Using Eqs. (A2), we can calculate the desired elements of the Green's function, avoiding the inversion of a matrix having the dimension of the full Fock space.

APPENDIX B: SCALING OF Δ_t

Asymptotic behavior of the scaling functions. In the ergodic phase, the scaling ansatz Eq. (3) reads

$$\ln\Delta_t = \ln\Delta_c + \mathcal{F}_{\rm vol}(\mathcal{N}_F/\Lambda),$$

with the critical $\Delta_c = C_c\mathcal{N}_F^{-(1-D_c)}$ and C_c a constant; equivalently,

$$\mathcal{F}_{\rm vol}\left(\frac{\mathcal{N}_F}{\Lambda}\right) = \ln\Delta_t - \ln C_c + (1-D_c)\ln\Lambda + (1-D_c)\ln\frac{\mathcal{N}_F}{\Lambda}. \tag{B1}$$

Deep in an ergodic phase, both Λ and Δ_t are $O(1)$. From Eq. (B1), for $x = \mathcal{N}_F/\Lambda \gg 1$ the asymptotic large-x behavior of $\mathcal{F}_{\rm vol}(x)$ is then

$$\mathcal{F}_{\rm vol}(x) \sim (1-D_c)\ln x \tag{B2}$$

up to $O(1)$ corrections. Its slope gives the fractal exponent $(1-D_c)$ for $W = W_c$, which is also found to be consistent with the numerical asymptotic fit in Fig. 1(b).

On the other hand, in the MBL phase $W > W_c$, $\Delta_t = C_m\mathcal{N}_F^{-(1-D_s)}$ [Fig. 1(b)], where C_m and D_s both depend on W. The scaling ansatz Eq. (3) then gives

$$\mathcal{F}_{\rm lin}\left(\frac{\ln\mathcal{N}_F}{\xi}\right) = \ln\frac{C_m}{C_c} - (1-D_c)\frac{\ln\mathcal{N}_F}{\xi}, \tag{B3}$$

with ξ defined as

$$\xi = \frac{(1-D_c)}{D_c - D_s}. \tag{B4}$$

As $D_s \to D_c^+$, i.e., as $W \to W_c^+$, we see that ξ diverges. Deep in the MBL phase, where $x = (\ln\mathcal{N}_F)/\xi \gg 1$, the asymptotic scaling is clearly

$$\mathcal{F}_{\rm lin}(x) \sim -(1-D_c)x. \tag{B5}$$

Finally, returning to the ergodic phase, Eq. (B1) with $x = \mathcal{N}_F/\Lambda$ can be cast as

$$\Delta_t = \Lambda^{-(1-D_c)}\exp[\mathcal{F}_{\rm vol}(x) - (1-D_c)\ln x + \ln C_c], \tag{B6}$$

where (as shown in the main text) the nonergodic volume $\Lambda \sim \exp[b/\sqrt{W_c - W}]$ is determined by W and C_c is a constant. For any $W < W_c$, and hence for any finite Λ no matter how large, the thermodynamic limit corresponds to $x \to \infty$. From Eq. (B2) the argument of the exponential in Eq. (B6) is then $O(1)$, so in the thermodynamic limit the order parameter Δ_t

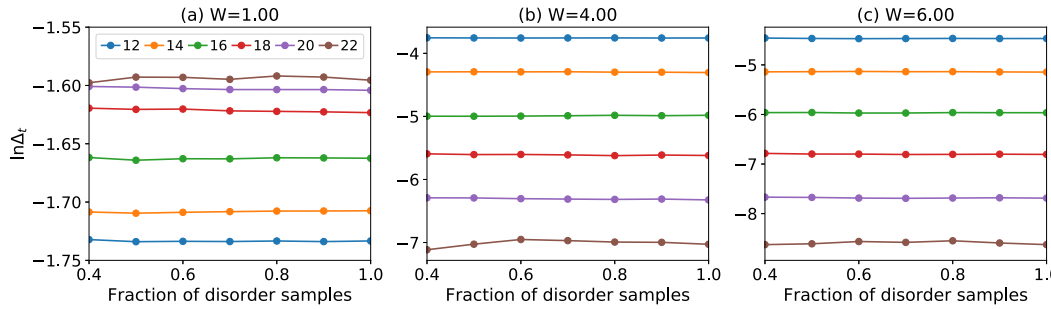

FIG. 8. Convergence of $\ln\Delta_t$ for different number of disorder samples, i.e., realizations. The maximum number of disorder samples used in these calculations are shown in Table I. For each system size the number of samples is varied from 0.4 times the maximum sample size to the maximum sample size. The convergence is tested for three disorder values $W = 1.0$ (in the thermal phase), 4.0 (near the transition), and 6.0 (in the MBL phase). Values of L corresponding to the colors are shown in the legend of (a).

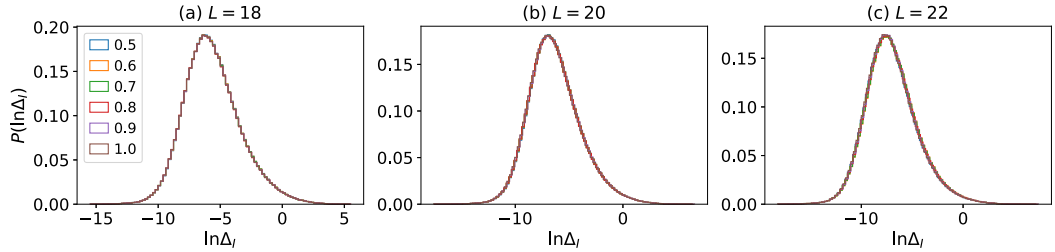

FIG. 9. Convergence of the distribution of $\ln\Delta_I$ for different sample sizes at disorder strength $W = 4.0$ near the transition. Similar to Fig. 7, the sample size is changed, as shown in the legend of (a), from 0.5 times the maximum sample size to the maximum sample sizes for all system sizes. For all sample sizes and system sizes considered, the distribution is seen to be the same.

vanishes continuously as

$$\Delta_t \sim \Lambda^{-(1-D_c)} \tag{B7}$$

and is controlled by Λ.

Dependence of scaling results on W_c. For the finite-size scaling shown in Fig. 2, $W_c = 3.75$ was employed. Figure 5 gives corresponding results for the scaling collapse on choosing $W_c = 3.5$ and 4. As seen, the quality of scaling is quite robust to the variation in W_c.

APPENDIX C: CONVERGENCE OF THE DATA WITH THE NUMBER OF FS SITES AND DISORDER REALIZATIONS

We first verify that the statistics of the imaginary part of the self-energy (Δ_I) is not affected by considering only the middle slice of the Fock space to generate the distribution. For both the ergodic and MBL phases, Fig. 6 gives a representative example of the fact that the distributions of Δ_I [$P(\Delta_I)$ or $P(\Delta_I/\eta)$] are barely affected whether one considers $I \in M$ or $I \in$ all Fock-space sites.

In Table I, we show the number of disorder realizations considered for different sizes to generate the distributions of diagonal elements of the Green's function. Due to finite computational time and resources, we follow the standard path of decreasing number of disorder realizations with increasing system size [17,20,25,35].

In Fig. 7, we show the relative change in the same quantity with respect to the value of $\ln\Delta_t$ for the largest sample size for all system sizes. The relative change is always less than 1% of the values plotted in Fig. 1(b), even for smaller sample sizes for all system sizes up to $L = 22$.

However, the quantity Δ_I is not expected to be self-averaging, i.e., there can be sample-to-sample fluctuations even in the thermodynamic limit. This kind of phenomenon is well known for conductance and its universal sample-to-sample fluctuations in studies [68,69] of single-particle Anderson localization. Still, a scaling theory for the Anderson localization transition can be constructed using the typical or average value of the conductance [69]. In a similar spirit, we consider the typical value of Δ_I, and find its value to be converged within the disordered realizations considered (Table I). We have also verified that the distributions do not change further with an increasing number of disorder realizations. Figure 8 shows the convergence of $\ln\Delta_t$ for different system sizes at three different disorder strengths, $W = 1.0$ (in the thermal phase), 4.0 (near the critical point), and 6.0 (in the MBL phase). The x axis represents the fraction of the maximum number of disorder samples considered for the calculation of $\ln\Delta_t$ as shown in Table I. For example, for $L = 18$ the disorder sample size is changed from 400 to 1000 in steps of 100.

Figure 9 shows the convergence of the distribution of $\ln\Delta_I$ over different samples and Fock space sites belonging to the middle slice, for system sizes $L = 18$, 20, and 22. We show here only the convergence for $W = 4.0$, although the convergence holds for all the disorder strengths. We would also like to emphasize that the typical value Δ_t for the local FS self-energy Δ_I is obtained by averaging over both disorder realizations and FS sites I in the middle slice of the FS lattice [Fig. 1(a)]. Since the number of sites in the middle slice increases exponentially with system size, the *effective* number of samples, albeit not independent, over which statistics is accumulated, is $\sim 10^6$ for $L \geqslant 14$; see Table I. This leads to Δ_t and $P(\ln\Delta_I)$ converging quite rapidly for larger system sizes like $L = 22$ even when the number of independent disorder realizations is smaller for larger L, as we demonstrate here.

[1] R. Nandkishore and D. A. Huse, Many-body localization and thermalization in quantum statistical mechanics, Annu. Rev. Condens. Matter Phys. **6**, 15 (2015).
[2] D. A. Abanin and Z. Papić, Recent progress in many-body localization, Ann. Phys. (Berlin) **529**, 1700169 (2017).
[3] F. Alet and N. Laflorencie, Many-body localization: An introduction and selected topics, C. R. Phys. **19**, 498 (2018).
[4] D. A. Abanin, E. Altman, I. Bloch, and M. Serbyn, Colloquium: Many-body localization, thermalization, and entanglement, Rev. Mod. Phys. **91**, 021001 (2019).
[5] J. M. Deutsch, Quantum statistical mechanics in a closed system, Phys. Rev. A **43**, 2046 (1991).
[6] M. Srednicki, Chaos and quantum thermalization, Phys. Rev. E **50**, 888 (1994).
[7] M. Srednicki, The approach to thermal equilibrium in quantized chaotic systems, J. Phys. A: Math. Gen. **32**, 1163 (1999).
[8] D. Basko, I. Aleiner, and B. Altshuler, Metal–insulator transition in a weakly interacting many-electron system with

localized single-particle states, Ann. Phys. (NY) **321**, 1126 (2006).

[9] I. V. Gornyi, A. D. Mirlin, and D. G. Polyakov, Interacting Electrons in Disordered Wires: Anderson Localization and Low-t Transport, Phys. Rev. Lett. **95**, 206603 (2005).

[10] J. Z. Imbrie, On many-body localization for quantum spin chains, J. Stat. Phys. **163**, 998 (2016).

[11] V. Oganesyan and D. A. Huse, Localization of interacting fermions at high temperature, Phys. Rev. B **75**, 155111 (2007).

[12] M. Žnidarič, T. Prosen, and P. Prelovšek, Many-body localization in the Heisenberg XXZ magnet in a random field, Phys. Rev. B **77**, 064426 (2008).

[13] A. Pal and D. A. Huse, Many-body localization phase transition, Phys. Rev. B **82**, 174411 (2010).

[14] J. H. Bardarson, F. Pollmann, and J. E. Moore, Unbounded Growth of Entanglement in Models of Many-Body Localization, Phys. Rev. Lett. **109**, 017202 (2012).

[15] J. A. Kjäll, J. H. Bardarson, and F. Pollmann, Many-Body Localization in a Disordered Quantum Ising Chain, Phys. Rev. Lett. **113**, 107204 (2014).

[16] M. Serbyn, Z. Papić, and D. A. Abanin, Criterion for Many-Body Localization-Delocalization Phase Transition, Phys. Rev. X **5**, 041047 (2015).

[17] D. J. Luitz, N. Laflorencie, and F. Alet, Many-body localization edge in the random-field Heisenberg chain, Phys. Rev. B **91**, 081103(R) (2015).

[18] P. T. Dumitrescu, A. Goremykina, S. A. Parameswaran, M. Serbyn, and R. Vasseur, Kosterlitz-thouless scaling at many-body localization phase transitions, Phys. Rev. B **99**, 094205 (2019).

[19] M. Kiefer-Emmanouilidis, R. Unanyan, M. Fleischhauer, and J. Sirker, Evidence for Unbounded Growth of the Number Entropy in Many-Body Localized Phases, Phys. Rev. Lett. **124**, 243601 (2020).

[20] J. Šuntajs, J. Bonča, T. c. v. Prosen, and L. Vidmar, Quantum chaos challenges many-body localization, Phys. Rev. E **102**, 062144 (2020).

[21] R. K. Panda, A. Scardicchio, M. Schulz, S. R. Taylor, and M. Žnidarič, Can we study the many-body localisation transition?, Europhys. Lett. **128**, 67003 (2020).

[22] D. Abanin, J. Bardarson, G. De Tomasi, S. Gopalakrishnan, V. Khemani, S. Parameswaran, F. Pollmann, A. Potter, M. Serbyn, and R. Vasseur, Distinguishing localization from chaos: Challenges in finite-size systems, Ann. Phys. (NY) **427**, 168415 (2021).

[23] P. Sierant, D. Delande, and J. Zakrzewski, Thouless Time Analysis of Anderson and Many-Body Localization Transitions, Phys. Rev. Lett. **124**, 186601 (2020).

[24] R. Modak and S. Mukerjee, Many-Body Localization in the Presence of a Single-Particle Mobility Edge, Phys. Rev. Lett. **115**, 230401 (2015).

[25] V. Khemani, D. N. Sheng, and D. A. Huse, Two Universality Classes for the Many-Body Localization Transition, Phys. Rev. Lett. **119**, 075702 (2017).

[26] A. Goremykina, R. Vasseur, and M. Serbyn, Analytically Solvable Renormalization Group for the Many-Body Localization Transition, Phys. Rev. Lett. **122**, 040601 (2019).

[27] A. Morningstar and D. A. Huse, Renormalization-group study of the many-body localization transition in one dimension, Phys. Rev. B **99**, 224205 (2019).

[28] A. Morningstar, D. A. Huse, and J. Z. Imbrie, Many-body localization near the critical point, Phys. Rev. B **102**, 125134 (2020).

[29] B. L. Altshuler, Y. Gefen, A. Kamenev, and L. S. Levitov, Quasiparticle Lifetime in a Finite System: A Nonperturbative Approach, Phys. Rev. Lett. **78**, 2803 (1997).

[30] D. E. Logan and S. Welsh, Many-body localization in Fock space: A local perspective, Phys. Rev. B **99**, 045131 (2019).

[31] S. Roy and D. E. Logan, Fock-space correlations and the origins of many-body localization, Phys. Rev. B **101**, 134202 (2020).

[32] A. Altland and T. Micklitz, Field Theory Approach to Many-Body Localization, Phys. Rev. Lett. **118**, 127202 (2017).

[33] S. Ghosh, A. Acharya, S. Sahu, and S. Mukerjee, Many-body localization due to correlated disorder in Fock space, Phys. Rev. B **99**, 165131 (2019).

[34] A. De Luca and A. Scardicchio, Ergodicity breaking in a model showing many-body localization, Europhys. Lett. **101**, 37003 (2013).

[35] N. Macé, F. Alet, and N. Laflorencie, Multifractal Scalings Across the Many-Body Localization Transition, Phys. Rev. Lett. **123**, 180601 (2019).

[36] S. Roy and D. E. Logan, Fock-space anatomy of eigenstates across the many-body localization transition, Phys. Rev. B **104**, 174201 (2021).

[37] G. De Tomasi, I. M. Khaymovich, F. Pollmann, and S. Warzel, Rare thermal bubbles at the many-body localization transition from the Fock space point of view, Phys. Rev. B **104**, 024202 (2021).

[38] E. Feenberg, A note on perturbation theory, Phys. Rev. **74**, 206 (1948).

[39] E. N. Economou, *Green's Functions in Quantum Physics* (Springer, Berlin, 2006).

[40] P. W. Anderson, Absence of diffusion in certain random lattices, Phys. Rev. **109**, 1492 (1958).

[41] R. Abou-Chacra, D. J. Thouless, and P. W. Anderson, A self-consistent theory of localization, J. Phys. C: Solid State Phys. **6**, 1734 (1973).

[42] E. N. Economou and M. H. Cohen, Existence of mobility edges in Anderson's model for random lattices, Phys. Rev. B **5**, 2931 (1972).

[43] D. C. Licciardello and E. N. Economou, Study of localization in Anderson's model for random lattices, Phys. Rev. B **11**, 3697 (1975).

[44] C. L. Bertrand and A. M. García-García, Anomalous Thouless energy and critical statistics on the metallic side of the many-body localization transition, Phys. Rev. B **94**, 144201 (2016).

[45] E. J. Torres-Herrera and L. F. Santos, Extended nonergodic states in disordered many-body quantum systems, Ann. Phys. (Berlin) **529**, 1600284 (2017).

[46] M. Serbyn, Z. Papić, and D. A. Abanin, Thouless energy and multifractality across the many-body localization transition, Phys. Rev. B **96**, 104201 (2017).

[47] F. Pietracaprina, N. Macé, D. J. Luitz, and F. Alet, Shift-invert diagonalization of large many-body localizing spin chains, SciPost Phys. **5**, 045 (2018).

[48] P. Sierant, M. Lewenstein, and J. Zakrzewski, Polynomially Filtered Exact Diagonalization Approach to Many-Body Localization, Phys. Rev. Lett. **125**, 156601 (2020).

[49] P. A. Lee and D. S. Fisher, Anderson Localization in Two Dimensions, Phys. Rev. Lett. **47**, 882 (1981).
[50] A. MacKinnon, The conductivity of the one-dimensional disordered Anderson model: a new numerical method, J. Phys. C **13**, L1031 (1980).
[51] A. MacKinnon and B. Kramer, The scaling theory of electrons in disordered solids: Additional numerical results, Z. Phys. B **53**, 1 (1983).
[52] I. García-Mata, O. Giraud, B. Georgeot, J. Martin, R. Dubertrand, and G. Lemarié, Scaling Theory of the Anderson Transition in Random Graphs: Ergodicity and Universality, Phys. Rev. Lett. **118**, 166801 (2017).
[53] N. Laflorencie, G. Lemarié, and N. Macé, Chain breaking and Kosterlitz-Thouless scaling at the many-body localization transition in the random-field Heisenberg spin chain, Phys. Rev. Research **2**, 042033(R) (2020).
[54] B. Bauer and C. Nayak, Area laws in a many-body localized state and its implications for topological order, J. Stat. Mech.: Theory Exp. (2013) P09005.
[55] S. Welsh and D. E. Logan, Simple probability distributions on a fock-space lattice, J. Phys.: Condens. Matter **30**, 405601 (2018).
[56] J. A. Verges, Computational implementation of the Kubo formula for the static conductance: application to two-dimensional quantum dots, Comput. Phys. Commun. **118**, 71 (1999).
[57] Prabhakar and A. Mukherjee, Fock space recursive Green's functions for bound complexes in partially filled bands of interacting systems, arXiv:2111.10781 [cond-mat.str-el].
[58] B. L. Altshuler, L. B. Ioffe, and V. E. Kravtsov, Multifractal states in self-consistent theory of localization: analytical solution, arXiv:1610.00758 [cond-mat.dis-nn].
[59] W. De Roeck and F. Huveneers, Stability and instability towards delocalization in many-body localization systems, Phys. Rev. B **95**, 155129 (2017).
[60] D. J. Luitz, F. Huveneers, and W. De Roeck, How a Small Quantum Bath Can Thermalize Long Localized Chains, Phys. Rev. Lett. **119**, 150602 (2017).
[61] I.-D. Potirniche, S. Banerjee, and E. Altman, Exploration of the stability of many-body localization in $d > 1$, Phys. Rev. B **99**, 205149 (2019).
[62] S. Bera, H. Schomerus, F. Heidrich-Meisner, and J. H. Bardarson, Many-Body Localization Characterized from a One-Particle Perspective, Phys. Rev. Lett. **115**, 046603 (2015).
[63] T. L. M. Lezama, S. Bera, H. Schomerus, F. Heidrich-Meisner, and J. H. Bardarson, One-particle density matrix occupation spectrum of many-body localized states after a global quench, Phys. Rev. B **96**, 060202(R) (2017).
[64] M. Hopjan and F. Heidrich-Meisner, Many-body localization from a one-particle perspective in the disordered one-dimensional Bose-Hubbard model, Phys. Rev. A **101**, 063617 (2020).
[65] M. Hopjan, F. Heidrich-Meisner, and V. Alba, Scaling properties of a spatial one-particle density-matrix entropy in many-body localized systems, Phys. Rev. B **104**, 035129 (2021).
[66] T. Orito and K.-I. Imura, Multifractality and Fock-space localization in many-body localized states: One-particle density matrix perspective, Phys. Rev. B **103**, 214206 (2021).
[67] A. Jana, V. R. Chandra, and A. Garg, Local density of states and scattering rates across the many-body localization transition, Phys. Rev. B **104**, L140201 (2021).
[68] P. A. Lee and A. D. Stone, Universal Conductance Fluctuations in Metals, Phys. Rev. Lett. **55**, 1622 (1985).
[69] K. Slevin, P. Markoš, and T. Ohtsuki, Reconciling Conductance Fluctuations and the Scaling Theory of Localization, Phys. Rev. Lett. **86**, 3594 (2001).